



Article

# Bioelectrocatalysis of Hemoglobin on Electrodeposited Ag Nanoflowers toward H<sub>2</sub>O<sub>2</sub> Detection

Ajay Kumar Yagati <sup>1,†</sup> , Hien T. Ngoc Le <sup>2,†</sup> and Sungbo Cho <sup>2,3,\*</sup>

<sup>1</sup> Institute of Analytical Chemistry, Chemo- and Biosensors, Universität Regensburg, 93053 Regensburg, Germany; ajay-kumar.yagati@ur.de

<sup>2</sup> Department of Electronics Engineering, Gachon University, Seongnam-si, Gyeonggi-do 13210, Korea; itnh1809@gachon.ac.kr

<sup>3</sup> Gachon Advanced Institute for Health Science & Technology, Gachon University, Incheon 21999, Korea

\* Correspondence: sbcho@gachon.ac.kr; Tel.: +82-31-750-5321; Fax: +82-31-750-5830

† These authors contributed equally to this work.

Received: 2 July 2020; Accepted: 13 August 2020; Published: 19 August 2020



**Abstract:** Hydrogen peroxide (H<sub>2</sub>O<sub>2</sub>) is a partially reduced metabolite of oxygen that exerts a diverse array of physiological and pathological activities in living organisms. Therefore, the accurate quantitative determination of H<sub>2</sub>O<sub>2</sub> is crucial in clinical diagnostics, the food industry, and environmental monitoring. Herein we report the electrosynthesis of silver nanoflowers (AgNFs) on indium tin oxide (ITO) electrodes for direct electron transfer of hemoglobin (Hb) toward the selective quantification of H<sub>2</sub>O<sub>2</sub>. After well-ordered and fully-grown AgNFs were created on an ITO substrate by electrodeposition, their morphological and optical properties were analyzed with scanning electron microscopy and UV–Vis spectroscopy. Hb was immobilized on 3-mercaptopropionic acid-coated AgNFs through carbodiimide cross-linking to form an Hb/AgNF/ITO biosensor. Electrochemical measurement and analysis demonstrated that Hb retained its direct electron transfer and electrocatalytic properties and acted as a H<sub>2</sub>O<sub>2</sub> sensor with a detection limit of 0.12 μM and a linear detection range of 0.2 to 3.4 mM in phosphate-buffered saline (PBS). The sensitivity, detection limit, and detection range of the Hb/AgNF/ITO biosensor toward detection H<sub>2</sub>O<sub>2</sub> in human serum was also found to be 0.730 mA mM<sup>-1</sup> cm<sup>-2</sup>, 90 μM, and 0.2 to 2.6 mM, indicating the clinical application for the H<sub>2</sub>O<sub>2</sub> detection of the Hb/AgNF/ITO biosensor. Moreover, interference experiments revealed that the Hb/AgNF/ITO sensor displayed excellent selectivity for H<sub>2</sub>O<sub>2</sub>.

**Keywords:** hemoglobin; silver nanoflower; hydrogen peroxide; electrochemical; biosensor

## 1. Introduction

Hydrogen peroxide (H<sub>2</sub>O<sub>2</sub>) is a reactive oxygen by-product that acts as a key regulator of various oxidative stress-related processes [1,2]. Moreover, it participates in pathways associated with rheumatoid arthritis [3], atherosclerosis [4,5], asthma [6,7], diabetic vasculopathy [8], and many neurodegenerative diseases [9]. Thus, creating a system for the accurate, sensitive, and selective determination of H<sub>2</sub>O<sub>2</sub> has been the goal of significant research effort [10]. In the past two decades, there has been a growing interest in the development of H<sub>2</sub>O<sub>2</sub> electrochemical biosensors based on the enzymatic activity of peptide-nanostructure-modified electrodes [11]. The utilization of nanoparticles (such as Au, Ag, Cu, and Fe) for the creation of nanostructures has received much attention because of their unique morphology, grain size, and physical, electrical, and magnetic properties that make them suitable for application in the fields of drug delivery [12], optoelectronics [13], energy storage elements [14], and microfluidics [15]. Many efforts have been made to synthesize materials characterized

by structural, compositional, and morphological uniformity, with a high surface to volume ratio allowing their application in various emerging fields [16]. Among these nanomaterials, Ag nanoparticles have been employed in a variety of applications because of their high extinction coefficient, large interfacial surface, and high thermal and electrical conductivity [17,18]. Moreover, Ag nanostructure-based plasmon biosensors have been shown to exhibit higher intensity wavelength-dependent plasmon bands in comparison with sensors based on Au and its conjugate structures [19]. Furthermore, surface modification chemistry has enabled the coupling of different biomaterials and inorganic materials, allowing their extensive utilization in developing biosensors [20,21].

Hemoglobin (Hb) is a Fe(II)-protoporphyrin IX (heme)-containing protein that contains the “globin fold” domain and reversibly binds molecular oxygen. It has a molar mass of approximately 67,000 g/mol and is composed of two  $\alpha$ - and two  $\beta$ -subunits, each containing one molecule of heme [22]. Hb is found in human erythrocytes (red blood cells) at a concentration of approximately 30% (w/v) or 20 mM (in heme). Among heme proteins, Hb is routinely used for the study of electron transfer reactions because of its commercial availability and low cost [23]. Because of its inherent peroxidase activity, Hb has been utilized as the basis for several  $\text{H}_2\text{O}_2$  sensors proposed in recent years. The direct electrochemistry of proteins immobilized on an electrode surface has been studied as a way to sensitively detect  $\text{H}_2\text{O}_2$  without the need for an additional electron transfer mediator. Earlier studies have reported the immobilization of Hb on various electrode surfaces, such as glassy carbon electrodes [24], metal oxides [25], nanoparticles [26], carbon dots [27], and graphene [28], for achieving direct electron transfer toward sensing applications. However, there is a constant quest to achieve more efficient biosensors, i.e., characterized by better sensitivity and shorter response times, by employing minimal fabrication steps.

In this study, we report the facile electrosynthesis of Ag nanoflowers (AgNF) on an indium tin oxide (ITO) electrode (AgNF/ITO). The surface morphology and the optical characteristics of the AgNFs were examined with scanning electron microscopy and UV–Vis spectroscopy, while the direct electron transfer by Hb immobilized on AgNF electrodes was investigated electrochemically. Based on our results, we propose the development of a sensitive electrochemical  $\text{H}_2\text{O}_2$  sensor based on Hb adsorbed on AgNF-modified ITO electrodes (Hb/AgNF/ITO). Figure 1 shows a schematic diagram summarizing the methodology we employed for creating our proposed modified electrode and its application toward  $\text{H}_2\text{O}_2$  detection.

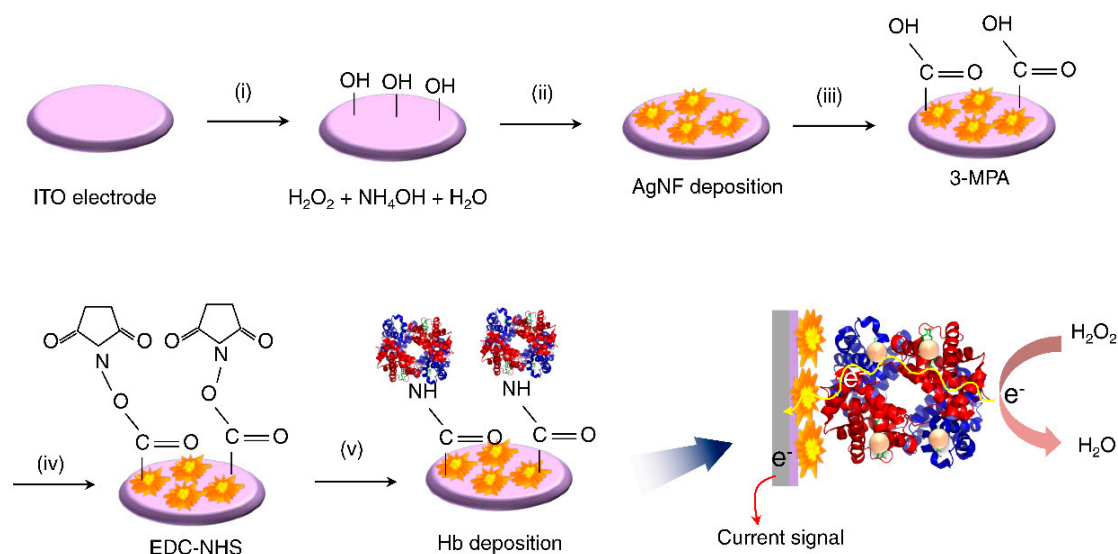


**Figure 1.** Schematic diagram depicting the surface modifications performed toward the formation of the Hb/AgNF/ITO electrode applied for  $\text{H}_2\text{O}_2$  detection.

## 2. Materials and Methods

### 2.1. Reagents

Human Hb, silver nitrate ( $\text{AgNO}_3$ ), polyethylene glycol (PEG) 200, *N*-(3-dimethylaminopropyl)-*N'*-ethylcarbodiimide hydrochloride (EDC), *N*-hydroxysuccinimide (NHS), 3-mercaptopropionic acid (3-MPA), uric acid (UA), L-ascorbic acid (AA), sodium nitrite ( $\text{NaNO}_2$ ), sodium bicarbonate ( $\text{NaHCO}_3$ ), and potassium nitrate ( $\text{KNO}_3$ ) were purchased from Sigma-Aldrich (St. Louis, MO, USA). Triton X-100 was purchased from GeorgiaChem (Smyrna, GA, USA), whereas  $\text{H}_2\text{O}_2$  was obtained from OCI Ltd. (Seoul, Korea) and diluted in deionized water for preparation of the desired molar concentrations. Phosphate-buffered saline (PBS; 10 mM phosphate, pH 7.4) was purchased from BioPrince (Gangwon, Korea). Buffer solutions were prepared using ultrapure deionized water ( $18.2 \text{ M}\Omega \text{ cm}^{-1}$ ) supplied by a Milli-Q system (Merck, Darmstadt, Germany). All other reagents were of analytical grade or of the highest purity available and used without any further purification unless stated otherwise.

### 2.2. Preparation of the Hb/AgNF/ITO Electrodes

ITO electrodes were initially cleaned by successive ultrasound treatments in Triton X-100: water (1:5, v/v) and ethanol, and were subsequently rinsed with DI water and dried under a  $\text{N}_2$  stream. The substrates were then treated in an oxidizing bath of  $\text{NH}_4\text{OH}:\text{H}_2\text{O}_2:\text{H}_2\text{O}$  (1:1:5, v/v) at  $80^\circ\text{C}$  for 40 min to remove particulate contaminants, washed thoroughly with DI water, and dried in a  $\text{N}_2$  stream.

The electrochemical deposition of AgNFs on bare ITO electrodes was performed in an aqueous solution of  $\text{AgNO}_3$  (1.0 mM in DI water) containing PEG 200 (20 mg/mL) as a surfactant by application of a voltage of  $-0.9 \text{ V}$  against a homemade  $\text{Ag}/\text{Ag}^+$  non-aqueous electrode (to avoid the precipitation of  $\text{AgCl}$  in the solution) for 50 s at a stable temperature of  $25^\circ\text{C}$ . The homemade  $\text{Ag}/\text{Ag}^+$  reference electrode was prepared by immersing the Ag wire in a solution of 1 mM of  $\text{Ag}^+$  (an aqueous solution of  $\text{AgNO}_3$ ) [17]. The deposition time of 50 s was chosen among three tested times (30, 50, and 80 s) because it produced the best results with respect to the formation of fully-grown AgNFs. The presence of PEG 200 acts as a surfactant and mild reducing agent to prevent the aggregation of Ag nanoparticles and to form AgNFs during the electrochemical deposition process. After deposition, the electrodes were cleaned with isopropyl alcohol to remove traces of the surfactant.

The AgNF/ITO electrodes were incubated with 50 mM of 3-MPA for 3 h to allow the formation of a self-assembled monolayer (SAM) from  $-\text{COOH}$  groups. The 3-MPA-modified electrodes were further incubated with EDC (0.4 M)/NHS (0.1 M) for 40 min (Figure 1). To allow the covalent binding of Hb on the activated surface, 20  $\mu\text{L}$  of a 0.1  $\text{mg mL}^{-1}$  Hb solution (pH 7.0) was drop-casted onto each electrode and kept in a humid chamber for 2 h to prevent drying of the surface during binding.

### 2.3. Apparatus and Measurements

UV-Vis absorption measurements on modified electrodes formed on an ITO-coated quartz substrate were performed with an Optizen Pop spectrophotometer (Mecasys, Daejeon, Korea). Both the AgNF substrate and the AgNF electrodes with adsorbed Hb were scanned from 300 to 800 nm at a scan speed of  $3 \text{ nm s}^{-1}$ . The EDC-NHS acts as a coupling to activate the  $\text{COOH}$  group of 3-MPA which binds with AgNFs and provides the strong amide group to link with Hb through the covalent bonding. Since the EDC-NHS coupling can be easily hydrolyzed at room temperature, the UV-Vis of Hb adsorbed AgNF without EDC-NHS coupling was measured. The surface topography of the electrodeposited surfaces was obtained by scanning electron microscopy (SEM) using an EM-30 microscope (COXEM, Daejeon, Korea) operated at a voltage of 20 kV. Surface-enhanced Raman scattering (SERS) is one of most commonly used optical measurement techniques for the in-situ monitoring of organic/inorganic materials at metal-metal and metal/liquid interfaces [29,30]. Ag, Au, Cu, and their conjugations, which are commonly deposited on substrates, produce very strong SERS signals. Thus, this method enables highly sensitive measurements of adsorbed molecules [31,32]. Raman spectroscopy was

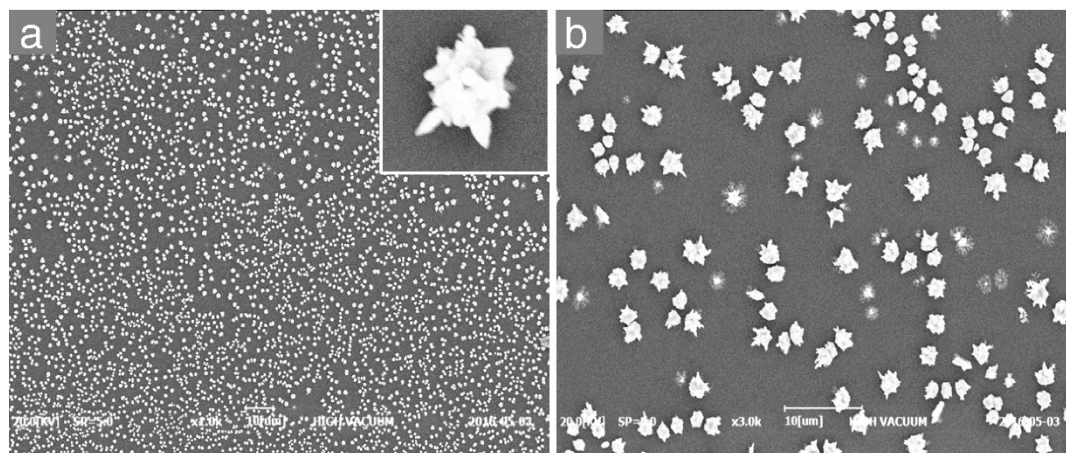
performed using a UniRAM spectrometer (UniNanoTech, Incheon, Korea) at a spatial resolution of 500 nm in the XY plane and 1  $\mu\text{m}$  in the Z-axis. Spectra were recorded using a laser emitting light at a wavelength of 532 nm. Several scans of 1 s from 500  $\text{cm}^{-1}$  to 2500  $\text{cm}^{-1}$  were recorded. Averages were calculated and used further.

Electrochemical measurements were performed with a CHI 660E electrochemical workstation (CH Instruments Inc., Austin, TX, USA) and an IVIUM CompactStat potentiostat (IVIUM Technologies, Eindhoven, the Netherlands) using modified substrate as the working electrode, a platinum wire as the counter electrode, and Ag/AgCl/KCl<sub>sat</sub> as the reference electrode. Electrochemical impedance spectroscopy (EIS) measurements were performed in 10 mM ferricyanide/ferrocyanide ((Fe(CN)<sub>6</sub>)<sup>3-/4-</sup>) with 0.1 M KCl as the background electrolyte. The input potential for EIS was 10 mV in amplitude with a frequency range of 0.1 to 10<sup>6</sup> Hz. The electrical properties of the electrodes were modeled with a modified Randles equivalent circuit using impedance-fitting analysis that was performed with the ZView software (Scribner Associates Inc., Southern Pines, NC, USA).

Amperometric (*I-t*) measurements on the Hb/AgNF/ITO electrode were performed using various H<sub>2</sub>O<sub>2</sub> concentrations. The potential was set at −0.5 V and *I-t* curves were recorded after successive additions of 10  $\mu\text{L}$  of 100 mM H<sub>2</sub>O<sub>2</sub> in 5 mL of 10 mM PBS (pH 7.0). Convective transport during amperometric determination was achieved with magnetic stirring at 1200 rpm. The chronoamperogram was recorded with N<sub>2</sub> purging to circumvent oxygen interference.

### 3. Results

Formation of AgNF structures on the ITO electrode by the electrodeposition process was observed by SEM and optical investigation. Figure 2 shows a topographic SEM image of the AgNFs fabricated on the ITO surface, revealing a uniform distribution over the entire surface and a size of around 800 nm. The number density of AgNFs was found to be 147 nanoflowers/ $\mu\text{m}^2$ , which was estimated using ImageJ analysis.



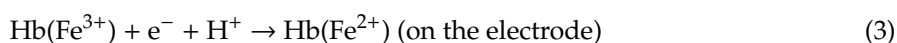
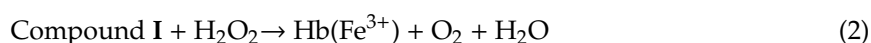
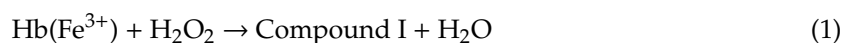
**Figure 2.** SEM images of (a) AgNFs electrodeposited on ITO surface (main) and a single nanoflower (inset), and (b) magnified view of the AgNFs shown in (a).

Figure 3a demonstrates the UV–Vis spectra of the Hb/AgNF/ITO and AgNF/ITO substrates. The AgNF/ITO substrate exhibits two surface plasmon absorption bands, a dominant broad feature in the visible range (674 nm) produced by the edge of the nanoflower, and a core-produced surface plasmon band at a shorter wavelength (497 nm). The Hb/AgNF/ITO substrate produces an additional shoulder peak at 358 nm caused by the M band of the heme group in hemoglobin, as well as bands corresponding to the electronic transitions of the aromatic amino acids of Hb. Raman spectroscopic analysis was performed on the electrodeposited electrodes, and the resulting spectra are shown in Figure 3b,c. Generally, the intensity of Raman signals is positively dependent on particle size [33], specific surface area [34], and the probability of SERS-active sites [35]. The spectrum of AgNF/ITO

electrodes displayed peaks at 642.7, 741.2, 930.7, 1058.59, 1380, 1587, 1774, 2124.25, and 2439  $\text{cm}^{-1}$ . Moreover, peaks at 1638.16, 1935.47, and 2336.29  $\text{cm}^{-1}$  were only observed in the Hb/AgNF/ITO spectrum and seemed to be caused by the vibrational modes of Hb. These data suggest that the silver nanoflower may be a good candidate for the formation of a SERS-active substrate.

Electrochemical impedance spectroscopy (EIS) is an efficient analytical method for studying the interfacial properties of a biosensor's electrode forming elements. Thus, to evaluate the formation of each deposition step toward the Hb/AgNF/ITO electrode, the EIS method was utilized to observe the variation in the impedance modulus of the electrode. Various modified ITO electrodes were analyzed, namely AgNF/ITO, 3-MPA/AgNF/ITO, EDC-NHS/AgNF/ITO, and Hb/AgNF/ITO electrodes. The corresponding Bode plots, in which the frequency was plotted against the impedance or the phase angles of each modified electrode, are presented in Figure 4a,b, respectively. The obtained impedance spectra were fitted to a Randles circuit model shown in the inset of Figure 4a. Stray capacitance ( $C_S$ ) was observed at a high-frequency range (above 1 MHz). The ohmic resistance of the electrolyte solution ( $R_S$ ), observed in the range of 100 kHz to 10 kHz, did not differ among the tested modified electrodes. The pseudo capacitive characteristics of the electrode interfacial impedance were observed at intermediate frequencies (100 Hz to 10 kHz for all modification processes) and were modeled as a constant phase element (CPE) with an impedance value of  $1/(CPE \cdot T \cdot (i\omega)^{CPE-P})$  [20], where  $i$  is the imaginary unit and  $\omega$  is the angular frequency. The actual electrode surface modifications could be analyzed at frequencies below 100 Hz, where the charge transfer resistance ( $R_{CT}$ ) corresponding to Warburg diffusion impedance ( $W_S$ ) was observed. The value of  $|Z|$  is dependent on the type of electrode surface modification (Figure 4a), which affects the CPE and  $R_{CT}$  values of the ITO electrode. The AgNF/ITO electrode had a lower  $|Z|$  value, i.e., a higher conductivity, compared to the bare ITO electrode, indicating that the increased surface area of the modified electrode allowed more  $(\text{Fe}(\text{CN})_6)^{3-/4-}$  ions to reach its surface. The immobilization of MPA on AgNF resulted in a higher  $|Z|$  value, indicating the formation of the SAM that prevented  $(\text{Fe}(\text{CN})_6)^{3-/4-}$  ions from reaching the electrode. However, the EDC-NHS activation led to a lower  $|Z|$  value, because the neutral amine bonds enabled more  $(\text{Fe}(\text{CN})_6)^{3-/4-}$  ions to reach the electrode compared to the  $-\text{COOH}$  groups. Finally, the Hb/AgNF/ITO electrode showed a greatly enhanced  $|Z|$ , indicating the complete blocking of  $(\text{Fe}(\text{CN})_6)^{3-/4-}$  ions from reaching the electrode. As seen in Figure 4b, the various electrodes also displayed distinct phase ( $\Phi$ ) vs. frequency ( $f$ ) plots. All types of electrodes (i.e., after any of the used modification processes) can be fitted into Randles equivalent circuits, which are utilized for understanding the interfacial properties of the electrodes [36]. The measured impedance data with fitted results were presented in Nyquist plot of Figure S1. The extrapolated parameters of the Randles circuit for each modification layer are presented in Table 1. The following  $R_{CT}$  values were calculated: bare ITO (49.5 k $\Omega$ ), AgNF/ITO (28.5 k $\Omega$ ), 3-MPA/AgNF/ITO (149.9 k $\Omega$ ), EDC-NHS/3MPA/ITO (83.8 k $\Omega$ ), and Hb/AgNF/ITO (879.7 k $\Omega$ ).

The electrocatalytic reduction of  $\text{H}_2\text{O}_2$  on Hb/AgNF/ITO electrodes was examined by Cyclic voltammetry (CV), and results are shown in Figure 5a. When  $\text{H}_2\text{O}_2$  was added to an electrochemical cell with a Hb/AgNF/ITO electrode, the reduction peaks were enhanced, whereas the oxidation currents completely disappeared due to an increase in the Hb-catalyzed reduction of  $\text{H}_2\text{O}_2$ . The successive addition of 10  $\mu\text{L}$  aliquots of 100 mM  $\text{H}_2\text{O}_2$  to a Hb/AgNF/ITO electrode immersed in 5 mL of PBS (10 mM) resulted in an increment in the cathodic peak current, which was attributed to  $\text{H}_2\text{O}_2$  reduction catalysis taking place on the surface of the modified electrode. These results reveal that the fabricated Hb/AgNF/ITO electrode had an excellent electrocatalytic activity toward  $\text{H}_2\text{O}_2$  detection. The mechanism of the Hb-catalyzed reduction can be broken down into the following reactions [37]:



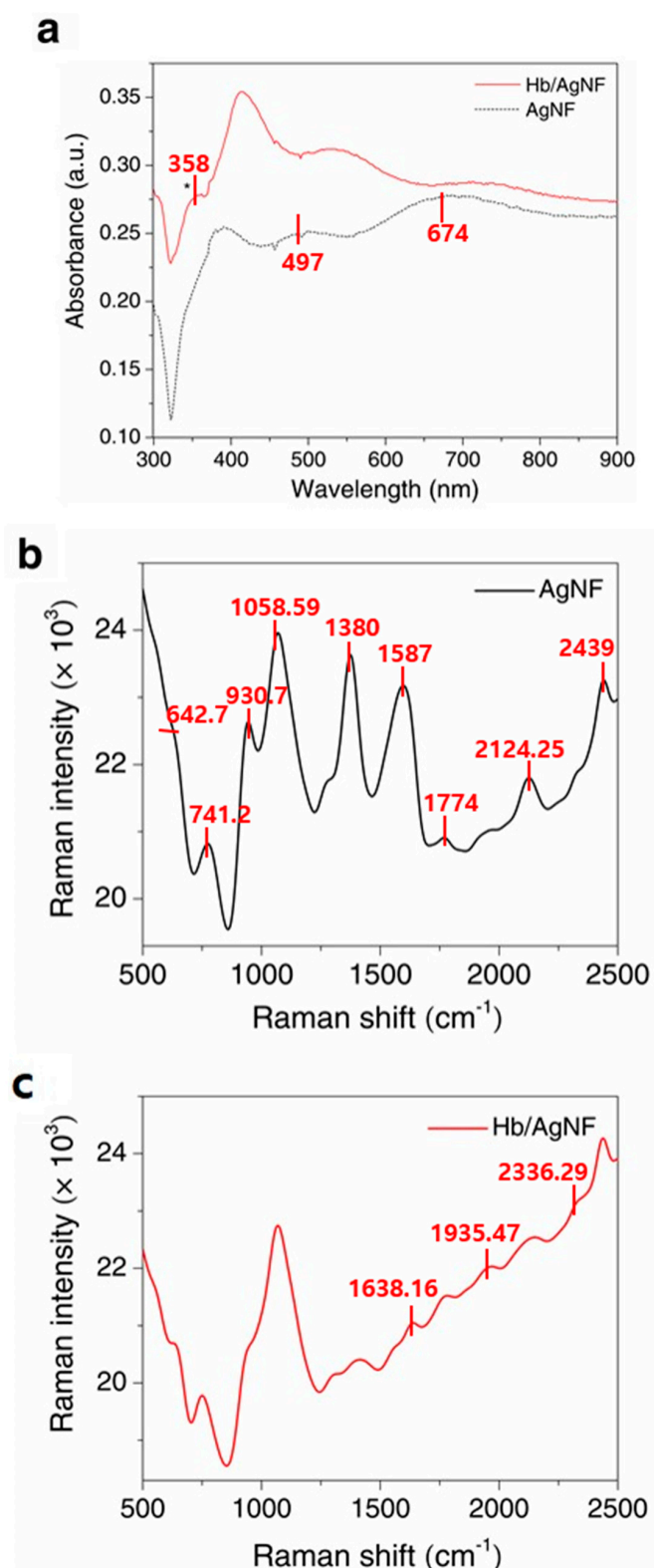
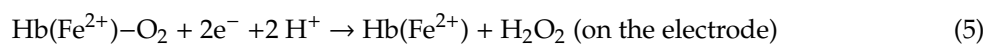
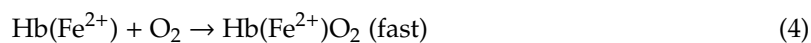


**Figure 3.** UV-Vis absorption spectra (a) and surface-enhanced Raman spectra (b) of AgNF/ITO and (c) Hb/AgNF/ITO substrates.

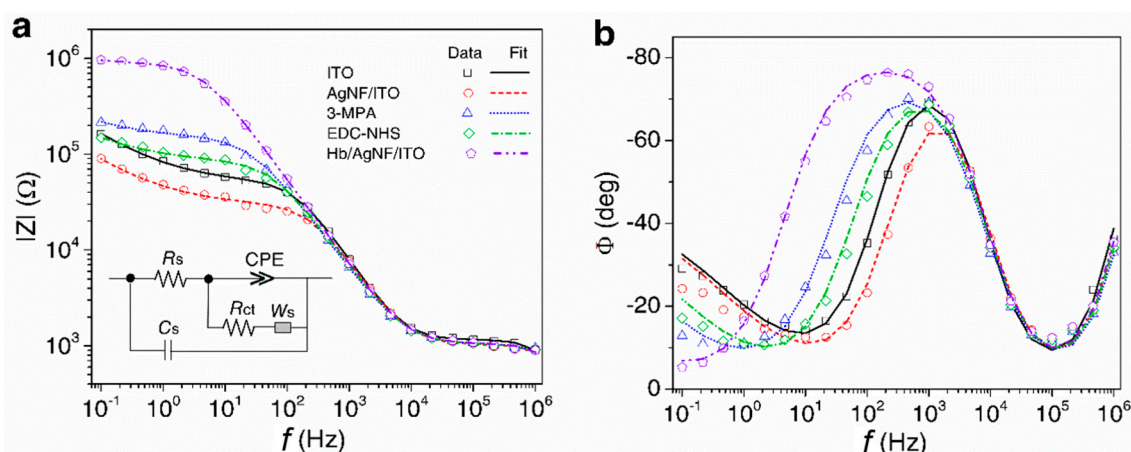


**Figure 4.** Bode plots of (a) impedance magnitude ( $|Z|$ ) and (b) phase ( $\Phi$ ) vs. frequency ( $f$ ) for bare ITO and AgNF/ITO electrodes, 3-MPA self-assembled monolayer (SAM) formation, EDC-NHS activation, and Hb binding. Measurements were performed in 10 mM  $(\text{Fe}(\text{CN})_6)^{3-/4-}$  with 0.1 M KCl as background electrolyte. The inset of (a) shows the modified Randles equivalent circuit used to fit the measured data.

**Table 1.** Extrapolated parameters from Randles circuits fitted with impedance data measured at each step of the electrode SAM formation shown in Figure 4a,b.

Electrodes	$R_s$ [ $\Omega$ ]	CPE-T ( $\times 10^{-9} \Omega^{-1} \text{s}^{\text{CPE-P}}$ )	CPE-P	$R_{CT}$ ( $\Omega$ )
ITO	$1161 \pm 10.25$	$31.97 \pm 1.46$	$0.947 \pm 0.005$	$49,562 \pm 594.47$
AgNF/ITO	$1035 \pm 20.74$	$41.63 \pm 4.81$	$0.921 \pm 0.012$	$28,577 \pm 715.05$
3-MPA	$1049 \pm 18.89$	$78.7 \pm 4.96$	$0.869 \pm 0.007$	$149,970 \pm 359.1$
EDC-NHS	$1040 \pm 19.49$	$64.5 \pm 4.82$	$0.885 \pm 0.008$	$83,884 \pm 1932$
Hb/AgNF/ITO	$1058 \pm 12.96$	$57.9 \pm 1.67$	$0.892 \pm 0.003$	$879,780 \pm 15,899$

The mechanism includes two catalytic cycles.  $\text{Hb}(\text{Fe}^{2+})$  reacts with  $\text{O}_2$  forming  $\text{Hb}(\text{Fe}^{2+})\text{O}_2$  (Equation (4)), which can receive two electrons on the electrode surface and revert to  $\text{Hb}(\text{Fe}^{2+})$  (Equation (5)). The  $\text{H}_2\text{O}_2$  produced in Equation (5) can induce or promote the catalytic cycles of Equations (4) and (5). Additionally, CVs of the AgNF/ITO electrode in absence and in presence of  $\text{H}_2\text{O}_2$  are shown in Supplementary Materials Figure S2. CV of AgNF/ITO in the absence of  $\text{H}_2\text{O}_2$  showed the oxidation peak at 0.4 V and broadening reduction peak around  $-0.4$ – $-0.55$  V of silver [38], and the oxidation peak of AgNF/ITO still appeared after 100 mM of  $\text{H}_2\text{O}_2$  was added into PBS solution, indicating no catalyzation of AgNF/ITO for  $\text{H}_2\text{O}_2$ .

Chronoamperometric (CA) measurements were performed to construct the current vs. time ( $I$ - $t$ ) curves on bare ITO, AgNF, and Hb/AgNF/ITO electrodes in order to elucidate the electrocatalytic response to  $\text{H}_2\text{O}_2$ . As seen in Figure 5b, the successive addition of  $\text{H}_2\text{O}_2$  to the Hb/AgNF/ITO electrode results in a clear increment in measured current. In contrast, no significant increment was observed when the same amount was added into AgNF/ITO or bare ITO electrodes. Specifically, bare ITO did not show any catalytic current toward the injected  $\text{H}_2\text{O}_2$ , whereas the AgNF/ITO electrode did show some response toward  $\text{H}_2\text{O}_2$ . This limited response can be attributed to the fact that AgNFs is an inorganic enzyme mimic displaying peroxidase-like activity [39]. However, the response current soon reached a plateau, and no further activity was observed. We concluded that, among the three electrodes, Hb/AgNF/ITO is the most stable and sensitive sensor of  $\text{H}_2\text{O}_2$  reduction because of the intrinsic activity of Hb toward  $\text{H}_2\text{O}_2$ . A response curve (Figure 5c) was obtained for concentrations of  $\text{H}_2\text{O}_2$  between 0.2 mM and 3.4 mM, which fell within the linear range. From the linear regression equation ( $y = -0.304x - 0.657$ ;  $R^2 = 0.996$ ), the sensitivity (slope of regression curve/area of the electrode) of the Hb/AgNF/ITO electrode toward  $\text{H}_2\text{O}_2$  was found to be  $0.956 \text{ mA mM}^{-1} \text{ cm}^{-2}$ . The detection

limit (LOD) was calculated at  $0.12 \mu\text{M}$  from the equation  $\text{LOD} = k \times \text{SD}_{\text{b.g.}}$ , where  $k$  is the signal to noise ratio and  $\text{SD}_{\text{b.g.}}$  is the standard deviation of the background signal [40].

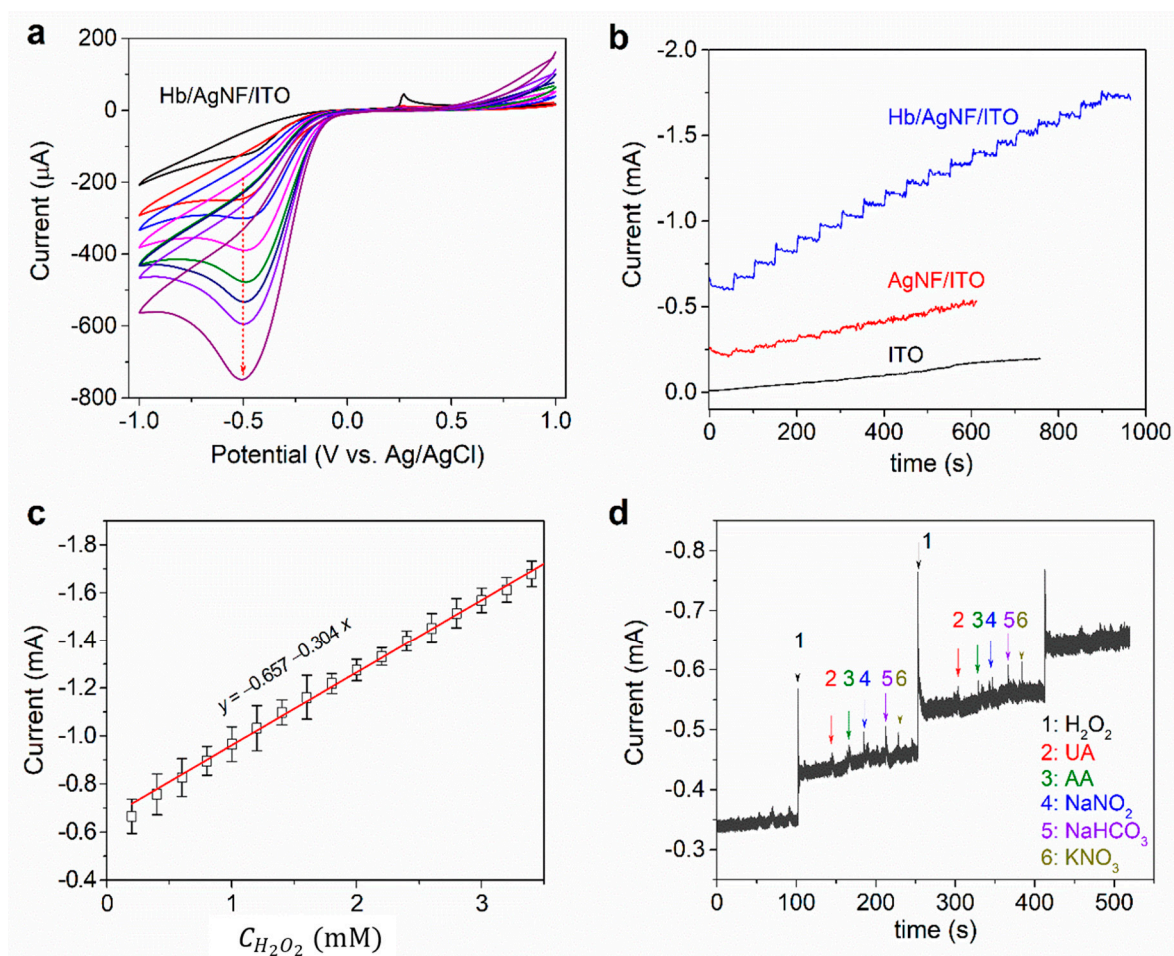


**Figure 5.** (a) Cyclic voltammetry (CV) curves obtained on the Hb/AgNF/ITO electrode upon successive additions of  $10 \mu\text{L}$  aliquots of  $100 \text{ mM}$   $\text{H}_2\text{O}_2$  in a  $5 \text{ mL}$  solution of  $10 \text{ mM}$  PBS ( $\text{pH}$  7.0) at a scan rate of  $50 \text{ mV/s}$ . The black line of CV presents the blank with no  $\text{H}_2\text{O}_2$ . (b) Chronoamperometric (CA) curves obtained for bare ITO, AgNF/ITO, and Hb/AgNF/ITO electrodes upon successive additions of  $10 \mu\text{L}$  aliquots of  $100 \text{ mM}$   $\text{H}_2\text{O}_2$  to  $5 \text{ mL}$  of  $10 \text{ mM}$  PBS with constant stirring ( $1200 \text{ rpm}$ ) at an applied potential of  $-0.5 \text{ V}$  vs. Ag/AgCl under nitrogen purging. (c) Calibration curve showing the concentration of  $\text{H}_2\text{O}_2$  ( $C_{\text{H}_2\text{O}_2}$ ) plotted vs. the measured catalytic peak current; data points express mean  $\pm$  SD of three replicated measurements, and the fitted curve represents a linear fit equation. (d)  $I-t$  curves obtained from a Hb/AgNF/ITO electrode at  $-0.5 \text{ V}$  upon successive additions to  $5 \text{ mL}$  PBS buffer ( $\text{pH}$  7.0) of  $5 \mu\text{L}$  aliquots of  $0.2 \text{ mM}$  uric acid (UA), L-ascorbic acid (AA), sodium nitrite ( $\text{NaNO}_2$ ), sodium bicarbonate ( $\text{NaHCO}_3$ ), and potassium nitrate ( $\text{KNO}_3$ ), along with  $5 \mu\text{L}$  of  $0.2 \text{ mM}$   $\text{H}_2\text{O}_2$ , with constant stirring.

To evaluate the practicability of the developed sensor, we checked the electrode's sensitivity in the presence of various interference compounds, such as ascorbic acid, uric acid, sodium nitrite, sodium bicarbonate, and potassium nitrate, at the concentration of  $0.2 \text{ mM}$ . The amperometric responses of the biosensor following consecutive injections of  $5 \mu\text{L}$  aliquots of  $0.2 \text{ mM}$   $\text{H}_2\text{O}_2$  and aliquots of the above mentioned interfering species are shown in Figure 5d. Measurements clearly show that the interfering species did not influence our biosensor's sensitivity to  $\text{H}_2\text{O}_2$ , indicating its high selectivity for  $\text{H}_2\text{O}_2$ . The stability of the sensor was also evaluated by examining its activity for 1 week. Results showed that the sensor retained its activity without degradation in its performance when kept

under 4 °C. The density of electroactive species in the surface ( $\Gamma_c$ ) was calculated to  $2.2 \times 10^{-4}$  mol/cm<sup>2</sup> from the slope of peak currents vs. scan rate plot of Supplementary Materials Figure S3 using the peak current equation [41]. Additionally, the Michaelis–Menten constant ( $K_m$ ) of Hb/AgNF/ITO was calculated to 0.63 from the slope of  $1/C_{H_2O_2}$  (mM<sup>-1</sup>) vs.  $1/I$  (mA<sup>-1</sup>) of the Lineweaver–Burk plot [42] in Supplementary Materials Figure S4, indicating the  $K_m$  of Hb/AgNF/ITO electrode has a lower value as compared to the  $K_m$  of free enzyme. In the physical meaning, the low  $K_m$  value represents the high enzyme activity, releasing the high sensitivity of the detection H<sub>2</sub>O<sub>2</sub>, in contrast to the high  $K_m$  off free enzyme in the comparison [43–46].

The clinical application of the Hb/AgNF/ITO sensor toward H<sub>2</sub>O<sub>2</sub> detection was explored in the human serum (HS) as shown in Figure 6. To avoid the matrix effect, pure HS was diluted 1:200 using 1 × PBS (pH 7.4). Various concentrations of H<sub>2</sub>O<sub>2</sub> (0.2–4.0 mM) in HS samples were prepared and applied for the CA measurement. Figure 6a shows the increasing of measured current in the addition of H<sub>2</sub>O<sub>2</sub> in HS to the Hb/AgNF/ITO electrode as well as in PBS (as shown in Figure 5b), indicating the nice electrocatalytic response to H<sub>2</sub>O<sub>2</sub> in HS of the Hb/AgNF/ITO sensor. A calibration curve was established from a linear range of concentration from 0.2 to 2.6 mM of H<sub>2</sub>O<sub>2</sub> in HS (Figure 6b) to express a linear regression equation ( $y = -0.021 - 0.232x$ ;  $R^2 = 0.996$ ). From this, the sensitivity of the Hb/AgNF/ITO sensor toward H<sub>2</sub>O<sub>2</sub> detection in HS was found to be 0.730 mA mM<sup>-1</sup> cm<sup>-2</sup>; the LOD was 90 μM, and the detection range was from 0.2 to 2.6 mM.

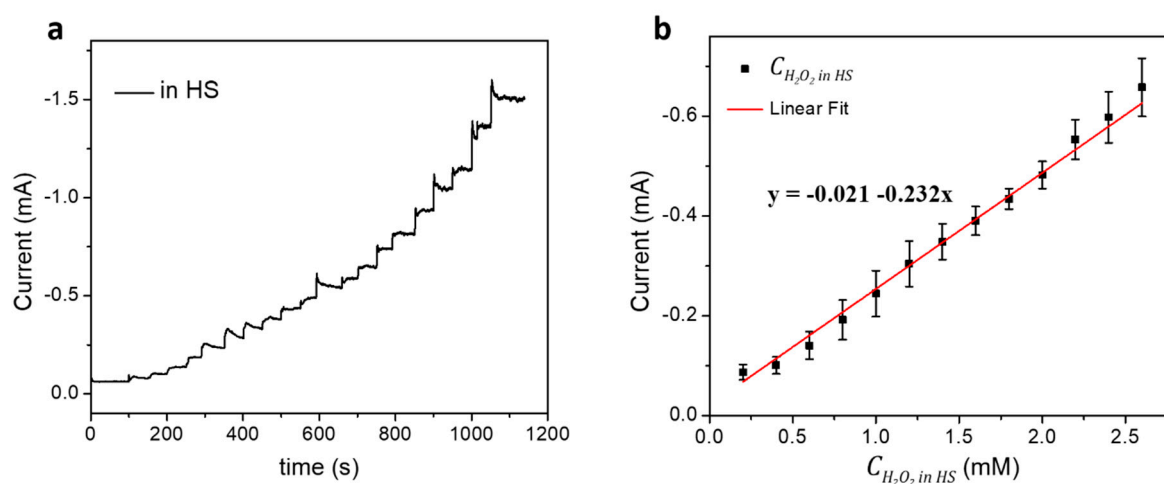


**Figure 6.** (a) CA ( $I-t$ ) curves obtained for Hb/AgNF/ITO electrode upon successive additions of 10 μL aliquots of 100 mM H<sub>2</sub>O<sub>2</sub> in human serum (HS) to 5 mL of 10 mM PBS with constant stirring (1200 rpm) at an applied potential of  $-0.5$  V vs. Ag/AgCl under nitrogen purging. (b) Calibration curve showing the concentration of H<sub>2</sub>O<sub>2</sub> in HS ( $C_{H_2O_2 \text{ in HS}}$ ) plotted vs. the measured catalytic peak current; data points express mean  $\pm$  SD of three replicated measurements and the fitted curve represents a linear fit equation.

Since the reproducibility and repeatability is a crucial factor for clinical application of the sensor, the relative standard deviations (RSDs) of the reproducibility and repeatability of the sensor were evaluated from data measured with three different sensors and from three replicate measurements, respectively. The RSDs of the reproducibility and repeatability of the sensor were found to 4.03% and 3.44%, respectively. The comparison of detection limit, detection range, and sensitivity of the developed biosensor were compared to the diverse nanostructure based-Hb immobilized sensors, as shown in Table 2.

**Table 2.** Comparison of selected quantities measured from Hb immobilized on modified electrodes toward H<sub>2</sub>O<sub>2</sub> detection.

Modified Electrode Sensors	Applied Potential (V) vs. Ag/AgCl	Detection Limit ( $\mu\text{M}$ )	Detection Range ( $\mu\text{M}$ )	Sensitivity ( $\mu\text{A mM}^{-1} \text{cm}^{-2}$ )	Reference
Hb/AgNPs BDDE <sup>a</sup>	−0.4	4.81	500 to 20,000	12.48	[47]
Hb/P123-NGP <sup>b</sup>	−0.4	8.24	10 to 150	-	[48]
Hb/Au/GR-CS/GCE <sup>c</sup>	−0.385	0.35	2 to 935	0.35	[49]
Hb/GCFME <sup>d</sup>	−0.5	2	8 to 214	1400	[50]
Hb-PAN <sup>e</sup> /GCE <sup>f</sup>	−0.25	8.3	8.3 to 500	-	[51]
Nafion/Hb/TiO <sub>2</sub> NPs <sup>g</sup> -rGO <sup>h</sup> /GCE	−0.35	0.01	0.1 to 140	-	[52]
Nafion/Hb-CS <sup>i</sup> -bBi <sub>2</sub> S <sub>3</sub> <sup>j</sup> /GCE	−0.4	0.096	0.4 to 4.8	-	[53]
Nafion/Hb/TiO <sub>2</sub> NS <sup>k</sup> -rGO/GCE	−0.35	0.01	0.1 to 145	-	[54]
Hb/AgNF/ITO	−0.5	0.12 (in PBS); 90 (in HS)	200 to 3400 (in PBS); 200 to 2600 (in HS)	956 (in PBS); 730 (in HS)	This work

<sup>a</sup> BDDE: Boron doped diamond electrode; <sup>b</sup> P123-NPG: Pluronic P123-nanographene platelet; <sup>c</sup> GR-CS: Graphene–chitosan; <sup>d</sup> GCFME: Graphene modified carbon fiber microelectrode; <sup>e</sup> PAN: Polyacrylonitrile; <sup>f</sup> GCE: Glassy carbon electrode; <sup>g</sup> TiO<sub>2</sub>NPs: Titanium oxide nanoparticles; <sup>h</sup> rGO: Reduced graphene oxide; <sup>i</sup> CS: Chitosan; <sup>j</sup> bBi<sub>2</sub>S<sub>3</sub>: Broccoli-like bismuth sulfide; <sup>k</sup> TiO<sub>2</sub>NS: Titanium oxide nanosheets.

#### 4. Conclusions

In conclusion, we developed an easy, simple, and cost-effective method for fabricating Hb/AgNFs/ITO-based H<sub>2</sub>O<sub>2</sub> sensors with excellent electrochemical catalytic activity and high selectivity. The proposed electrodeposition method achieved the uniform and reproducible formation of AgNFs on the ITO substrate. Optical and electrochemical measurements demonstrated that the AgNF depositions enhanced the measurement sensitivity as compared with bare electrodes. The H<sub>2</sub>O<sub>2</sub> amperometric sensor exhibited a sensitivity of 0.956 mA mM<sup>−1</sup> cm<sup>−2</sup> and a detection limit of 0.12  $\mu\text{M}$  in PBS. The sensor maintained a stable, sensitive, and excellent response for the detection of H<sub>2</sub>O<sub>2</sub> in the human serum with a sensitivity of 0.730 mA mM<sup>−1</sup> cm<sup>−2</sup> and a detection limit of 90  $\mu\text{M}$ . The proposed methodology could prove to be an efficient strategy and a promising platform for the study of protein electron transfer and the development of various biosensors.

**Supplementary Materials:** The following are available online at <http://www.mdpi.com/2079-4991/10/9/1628/s1>, Figure S1: Nyquist plot for bare ITO and AgNF/ITO electrodes, 3-MPA SAM formation, EDC-NHS activation, and Hb binding. Measurements were performed in 10 mM (Fe(CN)<sub>6</sub>)<sup>3−/4−</sup> with 0.1 M KCl as background electrolyte; Figure S2: CVs of AgNF/ITO electrode in absence and in presence of H<sub>2</sub>O<sub>2</sub> at a scan rate of 50 mV/s in 5 mL solution of 10 mM PBS (pH 7.0); Figure S3: (a) CV and (b) plot of peak currents vs. scan rate  $v$  of Hb/AgNF/ITO in the presence of 10 mM H<sub>2</sub>O<sub>2</sub> in 10 mM (Fe(CN)<sub>6</sub>)<sup>3−</sup> with 0.1 M KCl at different scan rate  $v$  from 50 to 175 mV/s; Figure S4: Lineweaver-Burk plot of 1/C<sub>H2O2</sub> (mM<sup>−1</sup>) vs. 1/I (mA<sup>−1</sup>).

**Author Contributions:** Writing—original draft preparation, A.K.Y., H.T.N.L.; methodology, A.K.Y., H.T.N.L.; writing—review and editing, supervision, S.C. All authors have read and agreed to the published version of the manuscript.

**Funding:** The work was supported by the National Research Foundation of Korea, Republic of Korea (Grant No. NRF-2018M3A9F1023690, 2019R1A2C1088680, and 2019R1G1A1100610) and by the GRRC program of Gyeonggi province (GRRC-Gachon2020(B01), AI-based Medical Image Analysis).

**Conflicts of Interest:** The authors declare no conflict of interest.

## References

1. Park, S.Y.; Je, J.Y.; Ahn, C.B. Phenolic Composition and Hepatoprotective Activities of *Allium Hookeri* Against Hydrogen-Peroxide-Induced Oxidative Stress in Cultured Hepatocytes. *J. Food Biochem.* **2016**, *40*, 284–293. [[CrossRef](#)]
2. Bekeschus, S.; Kolata, J.; Winterbourn, C.; Kramer, A.; Turner, R.; Weltmann, K.D.; Bröker, B.; Masur, K. Hydrogen peroxide: A central player in physical plasma-induced oxidative stress in human blood cells. *Free Radic. Res.* **2014**, *48*, 542–549. [[CrossRef](#)]
3. Mikuls, T.R.; O'Dell, J.R.; Ertl, R.; Bergman, D.A.; Rennard, S.I. Examining the exhaled levels of hydrogen peroxide in rheumatoid arthritis: A pilot study. *Ann. Rheum. Dis.* **2006**, *65*, 1252–1253. [[CrossRef](#)]
4. Hahn, D.M.; Chamseddine, A.H.; Miller, F.J. The effect of superoxide and hydrogen peroxide in atherosclerosis. *J. Investig. Med.* **2004**, *52*, 1081–1089. [[CrossRef](#)]
5. Park, J.G.; Oh, G.T. The role of peroxidases in the pathogenesis of atherosclerosis. *BMB Rep.* **2011**, *44*, 497–505. [[CrossRef](#)]
6. Teng, Y.; Sun, P.L.; Zhang, J.Y.; Yu, R.B.; Bai, J.L.; Yao, X.; Huang, M.; Adcock, M.I.; Barnes, P.J. Hydrogen Peroxide in Exhaled Breath Condensate in Patients with Asthma A Promising Biomarker? *Chest* **2011**, *140*, 108–116. [[CrossRef](#)] [[PubMed](#)]
7. Cristofari-Marquand, E.; Kacel, M.; Milhe, F.; Magnan, A.; Lehucher-Michel, M.P. Asthma caused by peracetic acid-hydrogen peroxide mixture. *J. Occup. Health* **2007**, *49*, 155–158. [[CrossRef](#)] [[PubMed](#)]
8. Rahimi, R.; Nikfar, S.; Larijani, B.; Abdollahi, M. A review on the role of antioxidants in the management of diabetes and its complications. *Biomed. Pharmacother.* **2005**, *59*, 365–373. [[CrossRef](#)] [[PubMed](#)]
9. Tabner, B.J.; Turnbull, S.; Fullwood, N.J.; German, M.; Allsop, D. The production of hydrogen peroxide during early-stage protein aggregation: A common pathological mechanism in different neurodegenerative diseases? *Biochem. Soc. Trans.* **2005**, *33*, 548–550. [[CrossRef](#)] [[PubMed](#)]
10. Kung, C.C.; Lin, P.Y.; Buse, F.J.; Xue, Y.H.; Yu, X.; Dai, L.M.; Liu, C.C. Preparation and characterization of three dimensional graphene foam supported platinum-ruthenium bimetallic nanocatalysts for hydrogen peroxide based electrochemical biosensors. *Biosens. Bioelectron.* **2014**, *52*, 1–7. [[CrossRef](#)]
11. Gong, Y.F.; Chen, X.; Lu, Y.L.; Yang, W.S. Self-assembled dipeptide-gold nanoparticle hybrid spheres for highly sensitive amperometric hydrogen peroxide biosensors. *Biosens. Bioelectron.* **2015**, *66*, 392–398. [[CrossRef](#)] [[PubMed](#)]
12. Ezhilarasu, H.; Vishalli, D.; Dheen, S.T.; Bay, B.H.; Srinivasan, D.K. Nanoparticle-Based Therapeutic Approach for Diabetic Wound Healing. *Nanomaterials* **2020**, *10*, 1234. [[CrossRef](#)] [[PubMed](#)]
13. Sergeev, M.M.; Zakoldaev, R.A.; Itina, T.E.; Varlamov, P.V.; Kostyuk, G.K. Real-Time Analysis of Laser-Induced Plasmon Tuning in Nanoporous Glass Composite. *Nanomaterials* **2020**, *10*, 1131. [[CrossRef](#)] [[PubMed](#)]
14. Thirupathi, A.R.; Sidhureddy, B.; Boateng, E.; Soldatov, D.V.; Chen, A. Synthesis and Electrochemical Study of Three-Dimensional Graphene-Based Nanomaterials for Energy Applications. *Nanomaterials* **2020**, *10*, 1295. [[CrossRef](#)]
15. Shen, J.; Shafiq, M.; Ma, M.; Chen, H. Synthesis and Surface Engineering of Inorganic Nanomaterials Based on Microfluidic Technology. *Nanomaterials* **2020**, *10*, 1177. [[CrossRef](#)] [[PubMed](#)]
16. Yagati, A.K.; Min, J.; Cho, S. Electrosynthesis of ERGO-NP Nanocomposite Films for Bioelectrocatalysis of Horseradish Peroxidase towards H<sub>2</sub>O<sub>2</sub>. *J. Electrochem. Soc.* **2014**, *161*, G133–G140. [[CrossRef](#)]
17. Yagati, A.K.; Choi, Y.; Park, J.; Choi, J.W.; Jun, H.S.; Cho, S. Silver nanoflower-reduced graphene oxide composite based micro-disk electrode for insulin detection in serum. *Biosens. Bioelectron.* **2016**, *80*, 307–314. [[CrossRef](#)]
18. Truong, T.T.V.; Kumar, S.R.; Huang, Y.T.; Chen, D.W.; Liu, Y.K.; Lue, S.J. Size-Dependent Antibacterial Activity of Silver Nanoparticle-Loaded Graphene Oxide Nanosheets. *Nanomaterials* **2020**, *10*, 1207. [[CrossRef](#)]
19. Liu, H.P.; Liu, T.Z.; Zhang, L.; Han, L.; Gao, C.B.; Yin, Y.D. Etching-Free Epitaxial Growth of Gold on Silver Nanostructures for High Chemical Stability and Plasmonic Activity. *Adv. Funct. Mater.* **2015**, *25*, 5435–5443. [[CrossRef](#)]
20. Yagati, A.K.; Pyun, J.C.; Min, J.; Cho, S. Label-free and direct detection of C-reactive protein using reduced graphene oxide-nanoparticle hybrid impedimetric sensor. *Bioelectrochemistry* **2016**, *107*, 37–44. [[CrossRef](#)]
21. Yagati, A.K.; Park, J.; Cho, S. Reduced Graphene Oxide Modified the Interdigitated Chain Electrode for an Insulin Sensor. *Sensors* **2016**, *16*, 109. [[CrossRef](#)] [[PubMed](#)]

22. Pierzynski, G.M.; Sims, J.T.; Vance, G.F. Soils and Environmental Quality. In *Handbook on Metalloproteins*; Bertini, I., Sigel, A., Sigel, H., Eds.; CRC Press: Boca Raton, FL, USA, 2001.
23. Yang, X.X.; Kanter, J.; Piety, N.Z.; Benton, M.; Vignes, S.M.; Shevkoplyas, S.S. A Simple, Rapid, Low-Cost Test for the Diagnosis of Sickle Cell Disease Using a Paper-Based Hemoglobin Solubility Assay. *Blood* **2012**, *120*, 245. [[CrossRef](#)]
24. Li, F.P.; Nie, M.Z.; He, X.L.; Fei, J.J.; Ding, Y.L.; Feng, B. Direct electrochemistry and electrocatalysis of hemoglobin on a glassy carbon electrode modified with poly(ethylene glycol diglycidyl ether) and gold nanoparticles on a quaternized cellulose support. A sensor for hydrogen peroxide and nitric oxide. *Microchim. Acta* **2014**, *181*, 1541–1549. [[CrossRef](#)]
25. Hosseinzadeh, R.; Moosavi-Movahedi, A.A.; Ghourchian, H. Electrochemistry and molecular modeling of the hemoglobin-benzene interaction with a nanocrystalline mixed metal oxide. *RSC Adv.* **2014**, *4*, 49128–49136. [[CrossRef](#)]
26. Wu, H.; Sun, B.J.; Huang, D.Q.; Liu, Y.T.; Zhang, H. Characterization, Direct Electrochemistry, and Electrocatalysis of Immobilized Hemoglobin on a Platinum Nanoparticle-Didodecyldimethylammonium Bromide Composite Film. *Anal. Lett.* **2016**, *49*, 556–567. [[CrossRef](#)]
27. Murru, F.; Romero, F.J.; Sánchez-Mudarra, R.; Ruiz, F.J.G.; Morales, D.P.; Capitán-Vallvey, L.F.; Salinas-Castillo, A. Portable Instrument for Hemoglobin Determination Using Room-Temperature Phosphorescent Carbon Dots. *Nanomaterials* **2020**, *10*, 825. [[CrossRef](#)] [[PubMed](#)]
28. Chen, L.; Xu, Z.R. A three-dimensional nickel-doped reduced graphene oxide composite for selective separation of hemoglobin with a high adsorption capacity. *RSC Adv.* **2016**, *6*, 56278–56286. [[CrossRef](#)]
29. Dong, L.H.; Guan, G.Z.; Wei, X.; Zhao, X.L.; Xv, M. Creating SERS hot spots on length adjustable AgVO<sub>3</sub> nanobelts. *J. Alloy. Compd.* **2016**, *677*, 12–17. [[CrossRef](#)]
30. Barbillon, G. Latest Novelties on Plasmonic and Non-Plasmonic Nanomaterials for SERS Sensing. *Nanomaterials* **2020**, *10*, 1200. [[CrossRef](#)]
31. Fazio, B.; D'Andrea, C.; Foti, A.; Messina, E.; Irrera, A.; Donato, M.G.; Villari, V.; Micali, N.; Maragò, O.M.; Gucciardi, P.G. SERS detection of Biomolecules at Physiological pH via aggregation of Gold Nanorods mediated by Optical Forces and Plasmonic Heating. *Sci. Rep.* **2016**, *6*, 26952. [[CrossRef](#)]
32. Ilkhani, H.; Hughes, T.; Li, J.; Zhong, C.J.; Hepel, M. Nanostructured SERS-electrochemical biosensors for testing of anticancer drug interactions with DNA. *Biosens. Bioelectron.* **2016**, *80*, 257–264. [[CrossRef](#)] [[PubMed](#)]
33. Pellow-Jarman, M.V.; Hendra, P.J.; Lehnert, R.J. The dependence of Raman signal intensity on particle size for crystal powders. *Vib. Spectrosc.* **1996**, *12*, 257–261. [[CrossRef](#)]
34. Srichan, C.; Ekpanyapong, M.; Horprathum, M.; Eiamchai, P.; Nuntawong, N.; Phokharatkul, D.; Danvirutai, P.; Bohez, E.; Wisitsoraat, A.; Tuantranont, A. Highly-Sensitive Surface-Enhanced Raman Spectroscopy (SERS)-based Chemical Sensor using 3D Graphene Foam Decorated with Silver Nanoparticles as SERS substrate. *Sci. Rep.* **2016**, *6*, 23733. [[CrossRef](#)] [[PubMed](#)]
35. Zoppi, A.; Trigari, S.; Margheri, G.; Muniz-Miranda, M.; Giorgetti, E. Gold nanostars as SERS-active substrates for FT-Raman spectroscopy. *RSC Adv.* **2015**, *5*, 8523–8532. [[CrossRef](#)]
36. Chinnadayala, S.R.; Park, J.; Abbasi, M.A.; Cho, S. Label-free electrochemical impedimetric immunosensor for sensitive detection of IgM rheumatoid factor in human serum. *Biosens. Bioelectron.* **2019**, *143*, 111642. [[CrossRef](#)]
37. Hui, N.; Gao, R.F.; Li, X.Q.; Sun, W.; Jiao, K. Direct Electrochemistry of Hemoglobin Immobilized in Polyvinylalcohol and Clay Composite Film Modified Carbon Ionic Liquid Electrode. *J. Brazil. Chem. Soc.* **2009**, *20*, 252–258. [[CrossRef](#)]
38. Choi, Y.J.; Luo, T.J.M. Electrochemical properties of Silver Nanoparticle Doped Aminosilica Nanocomposite. *Int. J. Electrochem.* **2011**, *2011*, 404937. [[CrossRef](#)]
39. Jiang, H.; Chen, Z.H.; Cao, H.Y.; Huang, Y.M. Peroxidase-like activity of chitosan stabilized silver nanoparticles for visual and colorimetric detection of glucose. *Analyst* **2012**, *137*, 5560–5564. [[CrossRef](#)]
40. Le, H.T.N.; Park, J.; Chinnadayala, S.R.; Cho, S. Sensitive electrochemical detection of amyloid beta peptide in human serum using an interdigitated chain-shaped electrode. *Biosens. Bioelectron.* **2019**, *144*, 111694.
41. Wang, J. *Analytical Electrochemistry*, 2nd ed.; Wiley: New York, NY, USA, 2000; p. 209.
42. Kamin, R.A.; Wilson, G.S. Rotating ring-disk enzyme electrode for biocatalysis kinetic studies and characterization of the immobilized enzyme layer. *Anal. Chem.* **1980**, *52*, 1198–1205. [[CrossRef](#)]

43. Gao, L.Z.; Zhuang, J.; Nie, L.; Zhang, J.; Zhang, Y.; Gu, N.; Wang, T.; Feng, J.; Yang, D.; Perrett, S.; et al. Intrinsic peroxidase-like activity of ferromagnetic nanoparticles. *Nat. Nanotechnol.* **2007**, *2*, 577–583. [[PubMed](#)]
44. Zhang, L.; Han, L.; Hu, P.; Wang, L.; Dong, S. TiO<sub>2</sub> nanotube arrays: Intrinsic peroxidase mimetics. *Chem. Commun.* **2013**, *49*, 10480–10482. [[CrossRef](#)] [[PubMed](#)]
45. Mu, J.; Wang, Y.; Zhang, L. Intrinsic peroxidase-like activity and catalase-like activity of Co<sub>3</sub>O<sub>4</sub> nanoparticles. *Chem. Commun.* **2012**, *48*, 2540–2542. [[CrossRef](#)] [[PubMed](#)]
46. Cai, K.; Lv, Z.C.; Chen, K.; Huang, L.; Wang, J.; Shao, F.; Wang, Y.; Han, H. Aqueous synthesis of porous platinum nanotubes at room temperature and their intrinsic peroxidase-like activity. *Chem. Commun.* **2013**, *49*, 6024–6026. [[CrossRef](#)] [[PubMed](#)]
47. Jiang, L.Y.; Hu, J.P.; Foord, J.S. Electroanalysis of Hydrogen Peroxide at Boron Doped Diamond Electrode Modified by Silver Nanoparticles and Haemoglobin. *Electrochim. Acta* **2015**, *176*, 488–496. [[CrossRef](#)]
48. Xu, X.X.; Zhang, J.X.; Guo, F.; Zheng, W.; Zhou, H.M.; Wang, B.L.; Zheng, Y.F.; Wang, Y.B.; Cheng, Y.; Lou, X.; et al. A novel amperometric hydrogen peroxide biosensor based on immobilized Hb in Pluronic P123-nanographene platelets composite. *Colloids Surface B* **2011**, *84*, 427–432. [[CrossRef](#)]
49. Zhang, L.L.; Han, G.Q.; Liu, Y.; Tang, J.; Tang, W.H. Immobilizing haemoglobin on gold/graphene-chitosan nanocomposite as efficient hydrogen peroxide biosensor. *Sens. Actuators B Chem.* **2014**, *197*, 164–171. [[CrossRef](#)]
50. Bai, J.; Wu, L.P.; Wang, X.J.; Zhang, H.M. Hemoglobin-graphene modified carbon fiber microelectrode for direct electrochemistry and electrochemical H<sub>2</sub>O<sub>2</sub> sensing. *Electrochim. Acta* **2015**, *185*, 142–147. [[CrossRef](#)]
51. Shan, D.; Wang, S.X.; Zhu, D.B.; Xue, H.G. Studies on direct electron transfer and biocatalytic properties of hemoglobin in polyacrylonitrile matrix. *Bioelectrochemistry* **2007**, *71*, 198–203. [[CrossRef](#)]
52. Liu, H.; Duan, C.Y.; Su, X.; Dong, X.N.; Shen, W.Q.; Zhu, Z.F. Titania nanoparticles modified reduced graphene oxide nanocomposite with a double-layered structure encapsulating hemoglobin for a mediator-free biosensor. *Ceram. Int.* **2014**, *40*, 9867–9874. [[CrossRef](#)]
53. Chen, X.Q.; Wang, Q.X.; Wang, L.H.; Gao, F.; Wang, W.; Hu, Z.S. Imidazoline derivative templated synthesis of broccoli-like Bi<sub>2</sub>S<sub>3</sub> and its electrocatalysis towards the direct electrochemistry of hemoglobin. *Biosens. Bioelectron.* **2015**, *66*, 216–223. [[CrossRef](#)] [[PubMed](#)]
54. Liu, H.; Duan, C.; Su, X.; Dong, X.; Huang, Z.; Shen, W.; Zhu, Z. A hemoglobin encapsulated titania nanosheet modified reduced graphene oxide nanocomposite as a mediator-free biosensor. *Sens. Actuators B Chem.* **2014**, *203*, 303–310. [[CrossRef](#)]



© 2020 by the authors. Licensee MDPI, Basel, Switzerland. This article is an open access article distributed under the terms and conditions of the Creative Commons Attribution (CC BY) license (<http://creativecommons.org/licenses/by/4.0/>).